Marine Micropaleontology 141 (2018) 31–41

Contents lists available at ScienceDirect

Marine Micropaleontology

journal homepage: www.elsevier.com/locate/marmicro

Research paper

A 450-kyr planktonic foraminiferal assemblage record of IODP site U1352 and its implications for the migration of the subtropical front in the south-west Pacific

YingYing Wu, Xuan Ding*, Ke Hu

School of Ocean Sciences, China University of Geosciences (Beijing), Beijing 100083, China

ARTICLE INFO

Keywords:
South-west Pacific
Subtropical front
Planktonic foraminifers
Sea surface temperature
Sea-level changes
Southland front

ABSTRACT

The Subtropical Front (STF) is one of the major ocean fronts in the south-west Pacific. The STF migration has a distinct but varying impact on the temperature change throughout the region. To improve our understanding on the history of the STF migration and the relationship between STF migration and global climate change, we have generated a 450-kyr record of sea surface temperature (SST) change at IODP Site U1352 located in the Canterbury Basin off New Zealand. Planktonic foraminiferal assemblages from the site were used to derive SST estimates. Comparisons of the planktonic foraminiferal assemblage and SST record of IODP Site U1352 with those of ODP Site 1119, DSDP Site 594 and core MD06-2986 allow us to reconstruct the spatial change of the STF over the last 450 kyr by locating the positions of its Southland Front (SF) section, which runs nearly parallel to the South Island's shoreline. The percentage of *Neogloboquadrina pachyderma* in the sum of *Nq. pachyderma* and *Nq. incompta* was below 40% at Sites IODP U1352, ODP 1119 and DSDP 594 during Marine Isotope Stage (MIS) 11c, MIS 7a–c and MIS 5e. Moreover, the SSTs of the three sites during these periods were similar and close to that of the present-day. This indicates that the three sites were covered by a Subtropical Water–Subantarctic Water (STW–SAW) mixture during these interglacials. IODP Site U1352 recorded a similar scenario during MIS 7e. In comparison with previous studies, the higher resolution record of IODP Site U1352 showed the influence of an STW–SAW mixture was limited to MIS 11c, MIS 7e, MIS 7a–c and MIS 5e at this site. The SSTs of Sites IODP U1352, ODP 1119 and DSDP 594 were similar during MIS 11a–b and MIS 9a–d. At the same time, the temperature differences among the three sites and core MD06-2986 (west of New Zealand) during MIS 11a–b and MIS 9a–d were larger than during interglacials MIS 11c, MIS 7a–c, and MIS 5e. These indicate that the Subantarctic Water (SAW) influenced Sites IODP U1352, ODP 1119 and DSDP 594 during MIS 11a–b and MIS 9a–d. The ~3–4 °C warmer SSTs at Sites IODP U1352 and ODP 1119 than at DSDP Site 594 suggest that the SF is situated between DSDP Site 594 and Sites IODP U1352, ODP 1119 during MIS 7d and glacial periods of MIS 10, MIS 8, and MIS 6. Hence, unlike previous studies in the region, MIS 7d is identified as a glacial period.

1. Introduction

The Canterbury Basin is located on the eastern margin of the South Island of New Zealand. Here the supply of sediment is through the fluvial systems that are linked to the Southern Alps, a 600 km chain of mountains along the Alpine fault plate boundary between the Pacific and Australian plates. The Southern Alps contain over 3000 glaciers that are larger than 0.01 km^2 (Clare et al., 2002). Such temperate maritime glaciers are very sensitive to climate perturbations owing to their high accumulation and ablation rates (Oerlemans and Fortuin, 1992). The mid-latitude location of the Southern Alps, in the path of the prevailing westerlies, at the junction between subtropical and polar air masses and near major ocean fronts such as the Subtropical Front (STF), adds even more to their sensitivity as a monitor of climatic change (Clare et al., 2002; Carter and Gammon, 2004).

In this region, most palaeoclimate studies have focused on the strength and interhemispheric timing of global and southern hemisphere climate cycles (e.g., Pahnke et al., 2003; Carter, 2005), and the behaviour of the surface water masses and ocean fronts (e.g., Fenner et al., 1992; Nelson et al., 1993; Wells and Okada, 1997; Weaver et al., 1998; Marret et al., 2001; Sikes et al., 2002; Sabaa et al., 2004; Scott and Hall, 2004; Crundwell et al., 2008). In the open oceans, surface water masses and fronts freely migrate towards the equator during cooling episodes and to the poles during warming episodes (Hayward

* Corresponding author.
E-mail address: dingx@cugb.edu.cn (X. Ding).

https://doi.org/10.1016/j.marmicro.2018.05.001
Received 11 April 2017; Received in revised form 2 May 2018; Accepted 5 May 2018
Available online 07 May 2018
0377-8398/

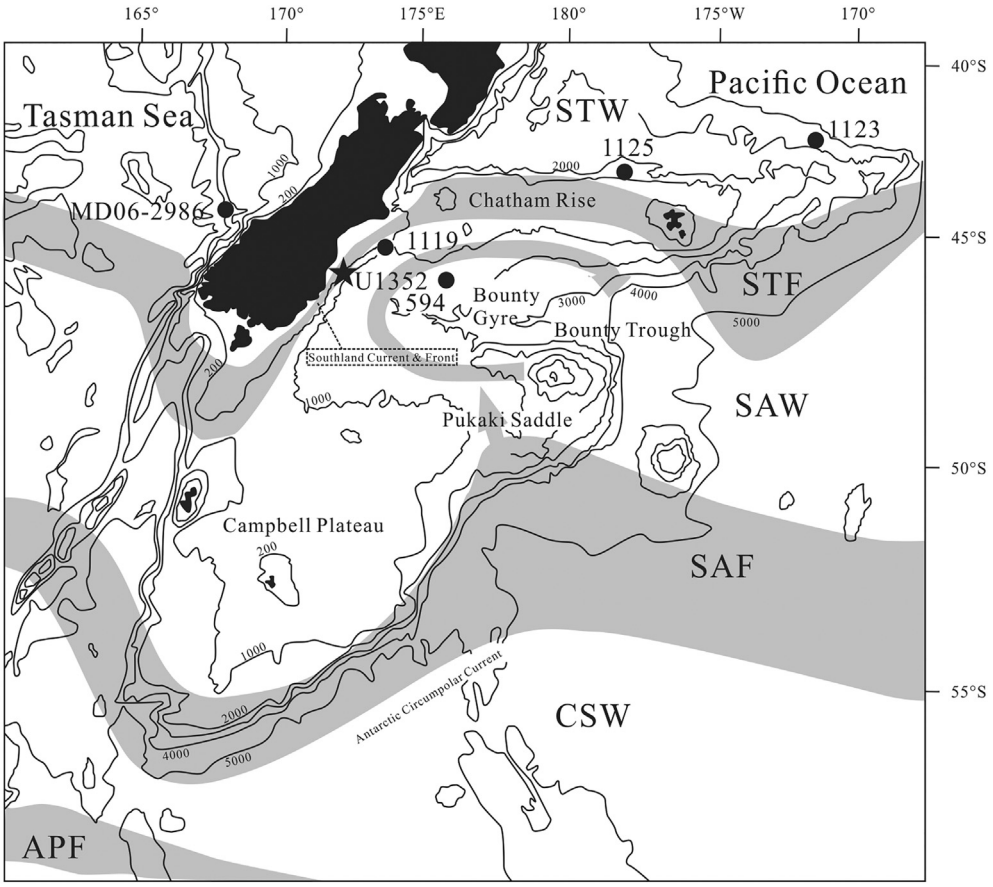

Fig. 1. Location of sites mentioned in the text, major bathymetric features, surface water masses and oceanic fronts of the southern New Zealand sector of the south-west Pacific (after Wilson et al., 2005). STW, Subtropical Water; STF, Subtropical Front; SAW, Subantarctic Water; SAF, Subantarctic Front; CSW, Circumpolar Surface Water; APF, Antarctic Polar Front.

et al., 2008; Hayward et al., 2012). In contrast, the expected northward migration of the fronts east of New Zealand during glacial periods was inhibited in this region by strong bathymetric control on their position (e.g., Fenner et al., 1992; Nelson et al., 1993, 2000; Weaver et al., 1998; Sikes et al., 2002; Carter et al., 2004; Schaefer et al., 2005; Wilson et al., 2005; Hayward et al., 2012). In the vicinity of ODP Site 1119 (Fig. 1), bathymetric and sea-level steering forces the front to move seaward during early glacial periods and move landward during late glacial and interglacial periods (Carter et al., 2004). This provides a unique perspective on the palaeoceanographic response to glacial–interglacial cycles. For example, present-day sea surface temperature (SST) at ODP Site 1119 (Fig. 1) is similar to that at DSDP Site 594. However, the SST at DSDP Site 594 was up to ~5 °C warmer during MIS 5e and ~3–4 °C cooler during glacial periods than at ODP Site 1119 (Wilson et al., 2005; Hayward et al., 2008).

Wilson et al. (2005) and Hayward et al. (2012) documented the migration of surface-water masses and fronts east of New Zealand on the basis of the SST records. They suggested that Sites ODP 1119 and DSDP 594 were immersed in the Subantarctic Water (SAW) during most of the interglacial periods, except for MIS 11 and MIS 5.5 when the southern edge of the STF migrated southward to overlie Sites ODP 1119 and DSDP 594. Wilson et al. (2005) inferred that the STF migrated offshore and was located between ODP site 1119 and DSDP site 594, and ODP Site 1119 was influenced by a Subtropical Water–Subantarctic Water (STW–SAW) mixture during most glacial periods. In contrast, Hayward et al. (2012) concluded that ODP Site 1119 was covered by SAW during most glacial periods except for MIS 4 and MIS 2. However, neither of the two studies is ideal due to the low sampling resolution of ODP Site 1119. With a high sampling resolution, IODP Site U1352, which is in the vicinity of ODP Site 1119, provides an opportunity to better constrain the temporal evolution of surface-water masses and fronts east of New Zealand and their relationships with palaeoclimate change.

In this study, we used planktonic foraminiferal census counts and the modern analogue technique (MAT) method to create a 450-kyr SST record for IODP Site U1352. The planktonic foraminiferal assemblage and SST records of IODP Site U1352 were then compared with those of three other sites (DSDP 594, ODP 1119 and MD06-2986; Fig. 1, Table 1) to determine the distribution of water masses off the east coast of the South Island over the last 450 kyr.

2. Oceanographic setting

The vast submarine margin of New Zealand strongly influences the distribution of major flows and oceanic fronts in the south-west Pacific (Heath, 1985). This is notably the case for the STF (Nelson et al., 2000) (Fig. 1). The STF is today characterised by a consistent gradient of 4 °C over < 0.5° of latitude and is currently distinguished by the 15 °C surface isotherm in summer, the 10 °C surface isotherm in winter and by the 34.7–34.8 surface salinity isopleth (Heath, 1985; Pahnke et al., 2003; Wilson et al., 2005; Pelejero et al., 2006; Li et al., 2010). To the east of New Zealand, the temperature range across the STF from south to north is generally 10–14 °C in winter and 14–18 °C in summer (Sikes

Table 1
Present-day location data for sites studied in this paper.

Site	Latitude	Longitude	Depth	Mean Ann. SST
IODP-U1352	44°56.26′S	172°01.36′E	344 m	11 °C
DSDP 594	45°31.41′S	174°56.88′E	1204 m	11 °C
ODP 1119	44°45.33′S	172°23.60′E	395 m	11 °C
MD06–2986	43°26.91′S	167°54.00′E	1477 m	15 °C
ODP 1123	41°47.17′S	171°29.94′W	3290 m	15.5 °C
ODP 1125	42°32.98′S	178°09.99′W	1365 m	14.5 °C

et al., 2002) while to the west of New Zealand, it is 8–12 °C in winter and 12–16 °C in summer (Li et al., 2010). To the south of the STF, the SAW is less saline (ca 34.5), nutrient-rich and cool, while to the north of the STF, the Subtropical Water (STW) is more saline (ca 35.7), nutrient-depleted and warm (Heath, 1985; Nelson et al., 2000; Shaw and Vennell, 2000; Sikes et al., 2002; Sutton, 2003; Pelejero et al., 2006; Li et al., 2010). In the open ocean to the west of New Zealand the STF hovers about 45°S, when it reaches the western shelf of the South Island it is deflected to the south around Stewart Island (Weaver et al., 1998; Wilson et al., 2005) (Fig. 1). The STF then runs northeast along the eastern South Island continental shelf to Chatham Rise where it swings to the east at ~44°S (Sutton, 2003; Wilson et al., 2005) (Fig. 1). The section of the STF that is bathymetrically locked to the shelf of the South Island's east coast is known as the Southland Front (SF), and the associated current is the Southland Current (SC) (Chiswell et al., 2015) (Fig. 1). The SC is composed of approximately 90% SAW and 10% STW, with the narrow band of inshore STW making inshore winter temperatures ~2 °C warmer than in the offshore band (Heath, 1972; Sutton, 2003). The two bands are separated by the SF (Sutton, 2003). Due to the SF's position, the movement of the SF reflects the migration of the STF and in turn climate changes in the region.

3. Materials and methods

3.1. Sampling and processing

Hole B at IODP Site U1352 (44°56.26′S, 172°1.36′E, water depth 344 m) was drilled on the continental slope south-east of New Zealand during IODP Expedition 317 (Fig. 1, Table 1; Expedition 317 Scientists, 2011). Only the upper 162 m CSF-A (core depth below seafloor; unless otherwise noted, all depths are given in CSF-A) of Hole U1352B was analysed for this study.

Hole U1352B samples were taken at 35–40 cm intervals, each sample with ~5–10 cm^3, and a total of 386 samples were obtained. After being dried and weighed, samples were soaked in deionised water without dispersant until completely dispersed, and then sieved and washed through a 63 μm-mesh sieve. The residue was dried at 40 °C followed by dry sieving to yield the coarse fraction with size over 150 μm.

3.2. Foraminiferal census data

The > 150 μm residue was repeatedly split until approximately 300 whole or nearly whole planktic foraminiferal tests remained. Samples with < 300 individuals in total were not split. The foraminifers in each split were identified and counted under a binocular microscope following the taxonomic concepts of Parker (1962), Imbrie and Kipp (1971), and Kipp (1976). The "*pachyderma-dutertrei* intergrade" category was not recognised. Right-coiling "*Neogloboquadrina pachyderma*" was identified throughout as *Neogloboquadrina incompta* following the work of Kucera (2007). The taxon *Neogloboquadrina pachyderma* was limited to sinistral-coiling forms.

3.3. Fragmentation index

The numbers of whole and fragmented (specimens < 50% complete) planktonic foraminiferal tests in the split of the coarse residue (> 150 μm) were counted to determine the planktonic foraminiferal fragmentation index (FI). The FI is a proxy for carbonate dissolution and was calculated using the formula of Le and Shackleton (1992).

$$FI\ (\%) = 100 \times (\text{number of fragments}/8)/(\text{number of fragments}/8 + \text{number of whole tests})$$

3.4. Foraminiferal accumulation rate

Foraminiferal accumulation rate (FAR) is a proxy for foraminiferal productivity. It takes account of differences in sedimentation rate, but makes no adjustments for taphonomic processes, such as dissolution or current removal or addition (Hayward et al., 2012).

FAR (n/kyr/cm^2) = dry bulk density (DBD) (g/cm^3) × absolute abundance of foraminifers (AAF) (n/g) × sedimentation rate (SR) (cm/kyr). DBD values of samples were obtained by linear interpolation between DBD value points of Hole U1352B from the Proceedings volume of IODP Expedition 317 (Expedition 317 Scientists, 2011). Then the FAR values of Hole U3152B were calculated.

3.5. Sea surface temperature estimation

The foraminiferal census data, excluding samples with planktonic foraminiferal specimens fewer than 250, were used to estimate the surface water palaeotemperature using the MAT 2.0 program (http://paleosofttools.usal.es). The Modern Analogue Technique (MAT) provides a reliable means of obtaining SST estimates from foraminiferal assemblages. It estimates SSTs to within 2.5 °C of the observed temperatures for the Southern Ocean foraminiferal records at 47°S and 51°S trap sites (King and Howard, 2003). In total, 160 sets of valid data were obtained, with 144 sets of data being in the interval 80–162 m and only 1 set of data in the interval 10–60 m. The temporal resolution in the SST record of U1352B is ~10.4 kyr for the interval of 0–80 m and ~2 kyr for the interval between 80 m and 162 m. The 122 samples containing 30–250 planktonic foraminiferal specimens were also used to estimate the surface water palaeotemperature but their results just provide a reference.

The advantages of the whole Southern Hemisphere data sets and the geographically constrained data sets have been discussed by Wilson et al. (2005) and Kucera et al. (2005), respectively. Here we use modern analogue data from the equator to 63°S. Faunas were obtained from Thiede et al. (1997, n = 63), Weaver et al. (1997, n = 35), Prell et al. (1999, n = 513), and Niebler et al. (2003, n = 201). Mean annual SSTs at a water depth of 0 m for the respective core sites were extracted from the World Ocean Atlas (https://www.nodc.noaa.gov/cgi-bin/OC5/woa13/woa13.pl). The database includes 812 core-top faunas, i.e., 79 fewer than the database of Crundwell et al. (2008). *Globorotalia crassaformis*, a species that has a regional extinction in the Indian Ocean, has not been removed from our census because it is still recorded in recent data (Bé, 1977; Wilson et al., 2005). The best modern analogues are identified using the squared chord distance to measure similarity. SSTs for the ten closest analogues were averaged to estimate the SST of the fossil assemblage. In order to compare SSTs of U1352B with those of other sites, notably Sites ODP 1119 (Wilson et al., 2005), DSDP 594 (Wilson et al., 2005) and MD06-2986 (Hayward et al., 2012), we applied the MAT 2.0 program and the same database to their respective planktonic foraminiferal data. The age models adopted for Sites ODP 1119 and DSDP 594 were the same as in Wilson et al. (2005). The chronostratigraphy for Site MD06-2986 followed that of Hayward et al. (2012).

4. Results

4.1. Age model

Based on four nannofossil biostratigraphic events and two Accelerator Mass Spectrometry (AMS) radiocarbon dates, Ding et al. (2017) established a refined age model for the upper 300 m CSF-A of Hole U1352B by correlating the planktonic (*Globigerina bulloides*) and benthic (*Nonionella flemingi*) $\delta^{18}O$ records with the EDC δD record on the AICC2012 time-scale (Jouzel et al., 2007; Bazin et al., 2013; Veres et al., 2013) and the stacked LR04 $\delta^{18}O$ record (Lisiecki and Raymo, 2005) (Fig. 2). The new 0.9 Ma age model of Hole U1352B established

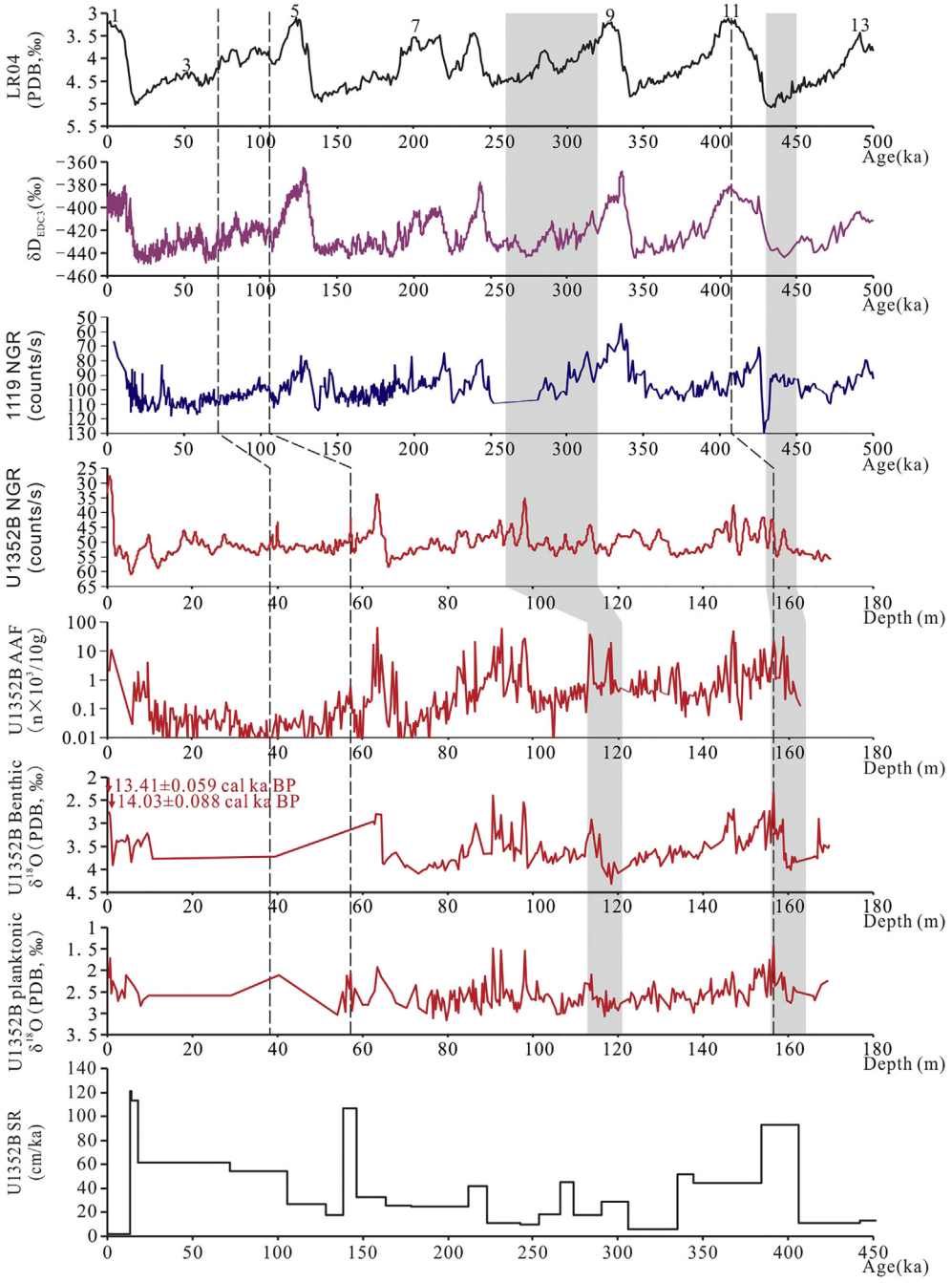

Fig. 2. Plots of the stacked LR04 ^{18}O standard curve (Lisiecki and Raymo, 2005), the EDC δD record on the AICC2012 time-scale (Bazin et al., 2013; Veres et al., 2013), the natural gamma radiation (NGR) of Sites ODP 1119 (Carter et al., 2004) and IODP-U1352, the absolute abundance of foraminifers (AAF) of U1352B, the benthic and planktonic foraminiferal $\delta^{18}O$ curves of U1352B. And the sedimentary rate curve of U1352B. Red arrows indicate the planktonic foraminiferal calibrated ^{14}C ages. Grey shadings mark the microfossil bioevents (Expedition 317 Scientists, 2011): Lowest occurrence (LO) *Emiliania huxleyi* (NN21 base), 0.29 (± 0.03) Ma, 112.82–121.1 m; Highest occurrence (HO) *Pseudoemiliania lacunosa* (NN20 base), 0.44 (± 0.01) Ma, 155.99–164.18 m. Dashed lines indicate the points modified from Ding et al. (2017). (For interpretation of the references to colour in this figure legend, the reader is referred to the web version of this article.)

by Ding et al. (2017) has a higher resolution than that of Hoyanagi et al. (2014). Therefore, the age model for the upper 162 m CSF-A of Hole U1352B in this study is based on that of Ding et al. (2017).

Two obvious peaks present at depths of 147.04 and 156.5 m, respectively, on the benthic $\delta^{18}O$ curve were considered as the peaks of MIS 11, which represent the ages of 406.03 ka and 425.09 ka, respectively (Ding et al., 2017). Nevertheless, we found the benthic $\delta^{18}O$ at a depth of 156.5 m is lighter than at a depth of 147.04 m, and the planktonic $\delta^{18}O$ record does not show an obvious peak at 147.04 m. This suggests that the peak at 156.5 m more likely corresponds to the peak at 406.03 ka in the EDC δD record on the AICC2012 time-scale (Jouzel et al., 2007; Bazin et al., 2013; Veres et al., 2013) (Fig. 2). We therefore adopted a revised age model for this interval (Table 2).

Due to the scarcity of $\delta^{18}O$ data, there is no tie point between 30 m to 60 m for the age models of Hole U1352B (Hoyanagi et al., 2014; Ding et al., 2017). Nevertheless, there exists fine correlation between the absolute abundance of foraminifers (AAF) and benthic $\delta^{18}O$ record in this hole (Fig. 2). By correlating the AAF with the EDC δD record on the AICC2012 time-scale (Jouzel et al., 2007; Bazin et al., 2013; Veres et al., 2013) and the stacked LR04 $\delta^{18}O$ record (Lisiecki and Raymo, 2005), two additional tie points were acquired at depths of 38.72 m and 57.1 m (Fig. 2, Table 2).

Depths were converted to ages by linear interpolation between stratigraphic control points. The age at a depth of 162.74 m was about 458.17 ka. Accordingly, the average sedimentation rate of the upper 162 m of Hole U1352B was 35.5 cm/kyr. The sedimentation rate was high during 406.03–384.05 kyr, 146.31–138.77 kyr and 18–13.41 kyr, with all being above 90 cm/kyr (Fig. 2, Table 2). This is followed by 384.05–335.22 kyr, 273.72–265.91 kyr, 223.39–211.87 kyr and 128.17–18 kyr, all above 40 cm/kyr (Fig. 2, Table 2).

Marine isotope stages may be further divided into substages. Here we use a recently recommended substage nomenclature (Railsback

Table 2
Table of control points and sedimentation rates for the Site U1352 age model.

CSF-A (m)	Age model of Ding et al. (2017) (ka)	Age model in this study (ka)	Sedimentation rate (cm/kyr)	Correlation
0.3	13.41	13.41	2.24	Calibrated ^{14}C age
1.05	14.03	14.03	120.97	Calibrated ^{14}C age
5.55	18	18	113.35	LR04
38.72	–	71.95*	61.48	EDC2012
57.1	–	105.66*	54.53	EDC2012
63.1	128.17	128.17	26.65	EDC2012
64.94	138.77	138.77	17.36	EDC2012
72.99	146.31	146.31	106.76	EDC2012
78.75	163.88	163.88	32.78	EDC2012
82.5	178.55	178.55	25.56	EDC2012
90.76	211.87	211.87	24.79	EDC2012
95.57	223.39	223.39	41.75	EDC2012
97.75	242.96	242.96	11.14	EDC2012
98.81	253.66	253.66	9.91	EDC2012
101.08	265.91	265.91	18.53	EDC2012
104.6	273.72	273.72	45.07	EDC2012
107.56	290.43	290.43	17.71	EDC2012
112.06	306.23	306.23	28.48	EDC2012
113.75	335.22	335.22	5.83	EDC2012
118.56	344.5	344.5	51.83	EDC2012
136.03	384.05	384.05	44.17	EDC2012
147.04	406.03	—[a]	93.13	EDC2012
156.5	425.09	406.03[a]	93.13	EDC2012
160.57	441.84	441.84	11.37	EDC2012
167.1	490.99	490.99	13.29	EDC2012

[a] Represents the modified point.

et al., 2015). The length of each interglacial is calculated using the "half-transition boundaries" method in Past Interglacials Working Group of PAGES (2016).

4.2. Characteristics of foraminiferal assemblage

Foraminifers occurred in all of the U1352B samples, and were well preserved. Under the microscope, foraminifers showed little evidence of mineralisation and infilling. The 160 U1352B samples (> 250 planktonic foraminifers) have an averaged FI of 0.16 ± 0.29%. For the 282 samples (> 30 planktonic foraminifers) of U1352B, the averaged FI was 0.20 ± 0.34%. This indicates that the weak carbonate dissolution in U1352B would not have affected the census data (Hayward et al., 2012). The AAF in the 386 samples of Hole U1352B fluctuated widely from 0 (3 individuals in 11.96 g sample) to 64 × 10^3 n/10 g (dry weight), with an average value of 2 ± 7 × 10^3 n/10 g (Fig. 3K, L).

The AAF value was high in the interglacial periods of MIS 11c (25 samples, 3 ± 5 × 10^3 n/10 g, maximum 23 × 10^3 n/10 g), MIS 9e (7 samples, 9 ± 15 × 10^3 n/10 g, maximum 38 × 10^3 n/10 g), MIS 7e (3 samples, 18 ± 13 × 10^3 n/10 g, maximum 28 × 10^3 n/10 g), MIS 7a–c (22 samples, 6 ± 13 × 10^3 n/10 g, maximum 59 × 10^3 n/10 g) and MIS 5e (11 samples, 8 ± 19 × 10^3 n/10 g, maximum 64 × 10^3 n/10 g) (Fig. 3K, L).

Due to its location close to the shore, the possible effect of terrigenous supply at Site U1352 needs to be accounted for, hence the FAR is considered. The FAR was found to fluctuate widely for the 386 samples of Hole U1352B, from 0 to 728 × 10^3 n/kyr/cm^2, with an average of 13 ± 53 × 10^3 n/kyr/cm^2 (Fig. 3M).

The FAR was high during MIS 11c (25 samples, 43 ± 77 × 10^3 n/kyr/cm^2, maximum 347 × 10^3 n/kyr/cm^2), MIS 7a–c (22 samples, 32 ± 79 × 10^3 n/kyr/cm^2, maximum 366 × 10^3 n/kyr/cm^2) and MIS 5e (11 samples, 23 ± 51 × 10^3 n/kyr/cm^2, maximum 165 × 10^3 n/kyr/cm^2) (Fig. 3M).

In total, 18 species were identified from the planktonic foraminiferal assemblages in U1352B. Only the 160 samples with planktonic foraminifera over 250 individuals will be discussed in detail. The 122 samples containing 30–250 planktonic foraminifers were only used to provide a reference. Species percentages in the 282 samples (> 30 planktonic foraminifers) of U1352B are very similar to those observed in the reliable 160 samples. Overall, the planktonic foraminifera recorded at U1352B constitute a typical Subantarctic assemblage (Crundwell et al., 2008). The 160 samples of U1352B are characterised by abundant *Globigerina bulloides*, *Nq. pachyderma*, *Nq. incompta*, *Gr. crassaformis*, and *Globorotalia inflata*, on average accounting for 54.9 ± 11.2%, 21.3 ± 13.0%, 5.0 ± 4.0%, 5.7 ± 4.4%, and 5.9 ± 4.0% of planktonic foraminifers and ranges of 21.8–80.4%, 1.8–61.0%, 0–19.7%, 0–24.3%, and 0.3–18.3%, respectively (Fig. 3B–F). The contributions of *Turborotalita quinqueloba*, *Globigerinita glutinata*, and *Neogloboquadrina dutertrei* are small, with averaged abundance being 1.9 ± 1.5%, 1.3 ± 1.0%, and 1.2 ± 1.1%, and ranges 0–7.9%, 0–5.1%, and 0–6.9%, respectively. *Globorotalia truncatulinoides*, *Globorotalia scitula*, *Globorotalia crassula*, *Orbulina universa*, *Globorotalia hirsuta*, *Trilobus sacculifer*, *Globigerinella aequilateralis*, *Globigerinoides ruber*, *Globigerina falconensis*, *Tenuitella iota*, and *Globigerinita uvula* are also recognised, but they form only a minor part of the assemblages.

Neogloboquadrina pachyderma is a polar–subantarctic taxon (Bé and Tolderlund, 1971; Reynolds and Thunell, 1986; Hemleben et al., 1989; Dieckmann et al., 1991; Johannessen et al., 1994; Capotondi et al., 2016). *Globigerina bulloides*, *Tb. quinqueloba*, and *Gt. glutinata* are eutrophic taxa (Tolderlund and Bé, 1971; Bé, 1977; Duplessy et al., 1981; Prell and Curry, 1981; Brock et al., 1992; Martinez et al., 1998; Pflaumann and Jian, 1999; Crundwell et al., 2008). *Trilobus sacculifer*, *Gs. ruber* and *Ge. aequilateralis* are subtropical taxa. *Neogloboquadrina dutertrei* is a subtropical and tropical taxon (Tolderlund and Bé, 1971). The distribution pattern of Neo*globoquadrina dutertrei* also reflects salinity and productivity variations in the Pacific (Parker and Berger, 1971; Cullen, 1981). *Neogloboquadrina incompta* and *Gr. inflata* are temperate (cool subtropical) taxa (Tolderlund and Bé, 1971; Bé, 1977; Thunell and Reynolds, 1984; Reynolds and Thunell, 1986; Pflaumann et al., 1996; Weaver et al., 1997; Pflaumann and Jian, 1999; Barrows et al., 2000; Cléroux et al., 2013). *Globorotalia crassaformis*, *Gr. truncatulinoides*, *Gr. scitula*, *Gr. crassula*, *Or. universa*, and *Gr. hirsuta* are subtropical–temperate taxa (Tolderlund and Bé, 1971; Bé, 1977; Crundwell et al., 2008; Cléroux et al., 2013).

The relative abundance of *Gg. bulloides* at Site U1352 was higher than in core MD06-2986 (Hayward et al., 2012), but agreed with the relative abundance observed in sediment traps south of the Chatham Rise (King and Howard, 2001) (Fig. 3B). *Globorotalia inflata* and *Nq. incompta* abundances at Site U1352 (Fig. 3F, D) were lower than in core MD06-2986 (Hayward et al., 2012) but agreed with the sediment trap observations (King and Howard, 2001). The relative abundance of *Nq. pachyderma* at Site U1352 (Fig. 3C), on the other hand, was higher than in both core MD06-2986 (Hayward et al., 2012) and the sediment traps south of the Chatham Rise (King and Howard, 2001). *Globorotalia truncatulinoides* and *Globorotalia scitula* abundances (160 samples, 0.9 ± 1.5%, range of 0–7.4%; 160 samples, 0.8 ± 1.2%, range of 0–7.1%) at Site U1352 (Fig. 3G, H) were lower than in core MD06-2986 (Hayward et al., 2012) and agreed with the data from sediment traps in the Subantarctic Zone (King and Howard, 2003).

4.3. Sea surface temperature

The mean annual SSTs for U1352B during the last 450 kyr varied between 5.7 °C and 11.9 °C with an average of 8.5 °C (Figs. 4 and 5). The mean annual SST standard deviations of the ten closest analogues for U1352B ranged from 0.7 to 2.5 °C (Fig. 4C), with an average of 1.4 °C. The differences between our results and the SST estimates of Hayward et al. (2008, 2012) using the Artificial Neural Network (ANN) are also shown in Fig. 4D.

There is a lack of SST data for part of MIS 6, MIS 5a–d, and MIS 4-2

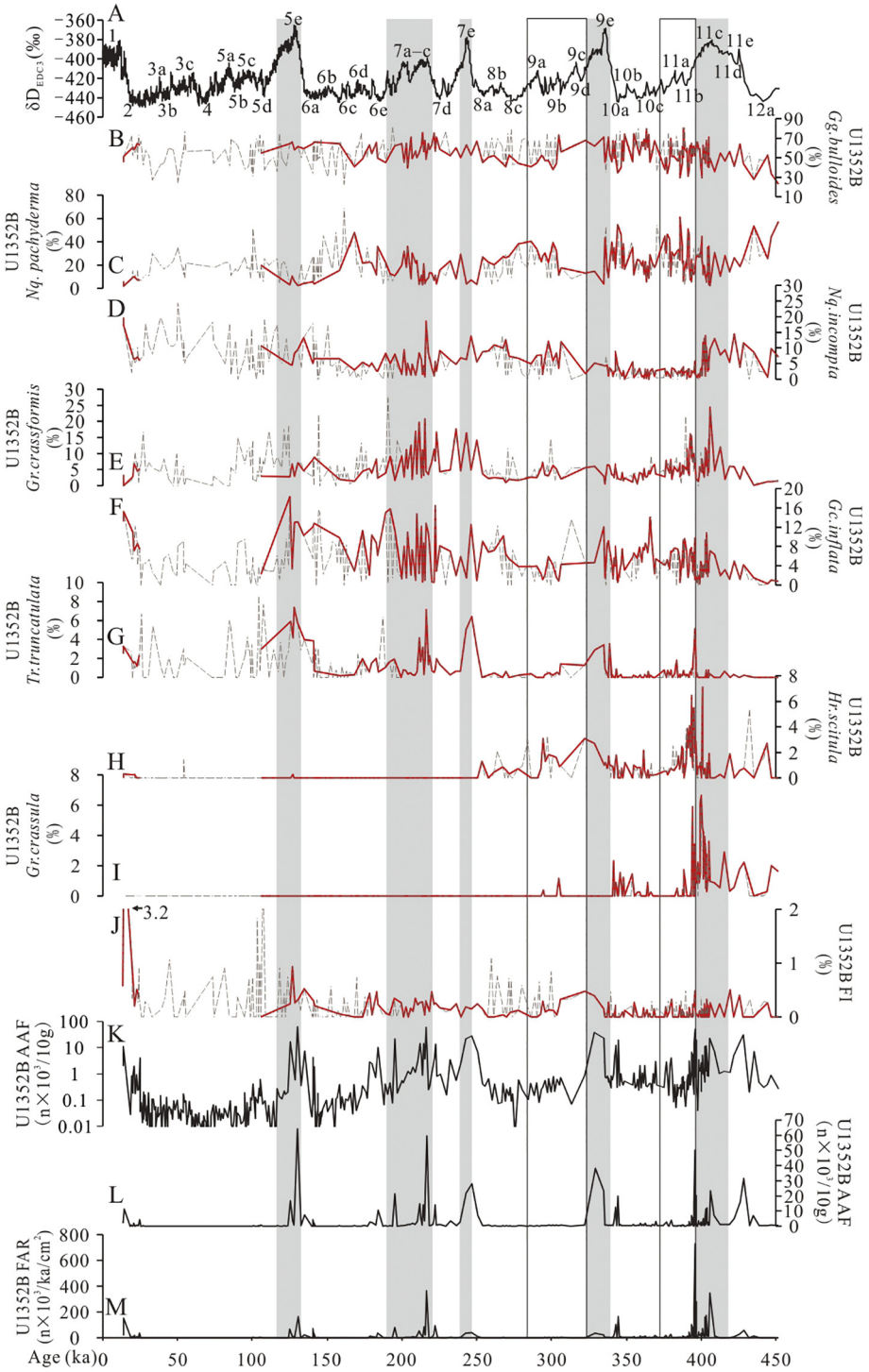

Fig. 3. (A) The EDC δD record on the AICC2012 time-scale (Bazin et al., 2013; Veres et al., 2013). (B–I) Relative abundance of the main planktic foraminiferal species. (J) The planktonic foraminiferal fragmentation index (FI). (K and L) The absolute abundance of foraminifers (AAF) of U1352B. (M) The foraminiferal accumulation rate (FAR) of U1352B. Black dashed line was samples of U1352B with > 30 planktonic foraminifers, red line was samples of U1352B with > 250 planktonic foraminifers. (For interpretation of the references to colour in this figure legend, the reader is referred to the web version of this article.)

due to the very low AAF. As shown in Figs. 4 and 5, the mean annual SST of U1352B was high during MIS 11c (22 samples, 8.6 ± 1.2 °C), MIS 7e (3 samples, 9.5 ± 2.5 °C), MIS 7a–c (19 samples, 9.0 ± 1.5 °C) and MIS 5e (4 samples, 11.1 ± 0.8 °C), with temperature peaks up to 11.2, 11.6, 11.7, and 11.9 °C, respectively. This was followed by MIS 9e (6 samples, 8.7 ± 1.2 °C), when SST peaked at 10.3 °C (Figs. 4 and 5). SSTs of U1352B were cooler during MIS 11b–MIS 10 (55 samples, 7.9 ± 0.9 °C) and MIS 9d–MIS 8 (19 samples, 8.0 ± 1.1 °C), but with temperature reaching up to 9.8 and 10.7 °C, respectively (Figs. 4 and 5).

5. Discussion

We compared the planktonic foraminiferal assemblage records and SST curves of Sites IODP U1352, ODP 1119, DSDP 594, and core MD06-2986 (estimated with the same MAT database) to determine the distribution of water masses around the South Island over the past 450 kyr.

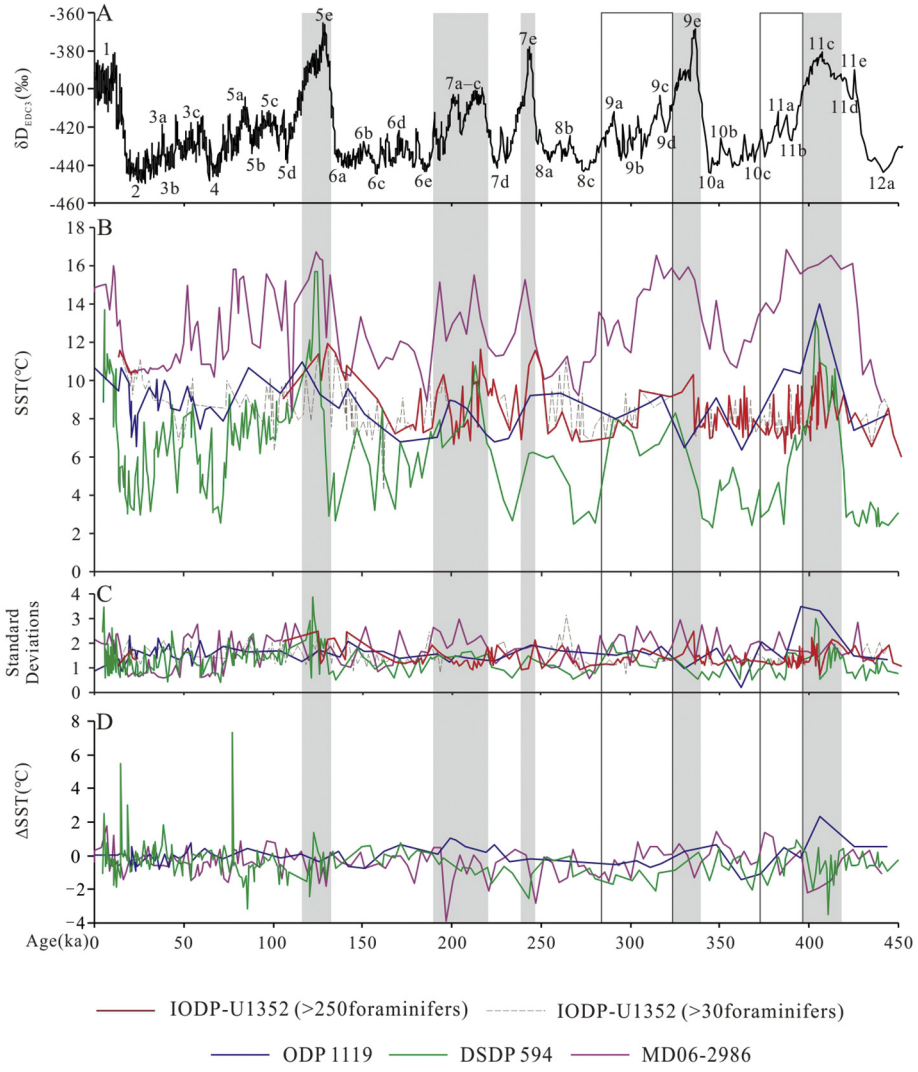

Fig. 4. (A) The EDC δD record on the AICC2012 time-scale (Bazin et al., 2013; Veres et al., 2013). (B) Mean annual sea surface temperature (SST) estimates of Sites IODP U1352, ODP 1119, DSDP 594 and MD06-2986 for the last 450 kyr. (C) The standard deviations in the mean annual SST estimation of Sites IODP U1352, ODP 1119, DSDP 594 and MD06-2986 for the last 450 kyr. (D) Differences between our results and the SST estimates of Hayward et al. (2008, 2012) using the Artificial Neural Network (ANN).

Based on the reconstructed SF migration, we attempt to establish a relationship between the STF migration and global climate change.

5.1. Migration of the Southland front in the interglacial periods

5.1.1. MIS 11c, MIS 9e, MIS 7e, MIS 7a–c, and MIS 5e

Studies around New Zealand have shown that the relative abundances of several planktonic species are good proxies for the location of the STF today (Hayward et al., 2012). One of the most reliable indicators is the percentage of *Nq. pachyderma* in the sum of *Nq. pachyderma* and *Nq. incompta* which lies between 20% and 40% for the STF (Nelson et al., 1993; Scott and Hall, 2004; Wilson et al., 2005; Hayward et al., 2012). The proportion is lower in the north than the south of the STF. The minimum proportion of *Nq. pachyderma* at Sites IODP U1352, ODP 1119 (Wilson et al., 2005) and DSDP 594 (Wilson et al., 2005) during MIS 11c and MIS 5e, and at Sites IODP U1352 and DSDP 594 (Wilson et al., 2005) during MIS 7a–c decreased to below 40% (Fig. 5E). The minimum proportion of *Nq. pachyderma* was not below 40% at ODP Site 1119 during MIS 7a–c (Wilson et al., 2005), whereas the adjacent IODP Site U1352 did capture this detail, which is possibly related to the higher temporal resolution of the latter. Therefore, our current data suggest that the SF was located over, or south of Sites IODP U1352, ODP 1119 and DSDP 594 during MIS 11c, MIS 7a–c and MIS 5e. Recent studies have also shown that the dominance of *Gr. inflata* over *Gg. bulloides* is a clear indicator of subtropical waters (King and Howard, 2001; Wilson et al., 2005; Hayward et al., 2012). However, *Gr. inflata* at IODP Site U1352 did not dominate over *Gg. bulloides* and its abundance was not as high as those to the north of the present-day STF (35.4%; Niebler and Gersonde, 1998) during MIS 11c, MIS 7a–c and MIS 5e (Figs. 3 and 5). Wilson et al. (2005) also inferred that *Gr. inflata* at ODP Site 1119 and DSDP Site 594 did not dominate over *Gg. bulloides* during MIS 11. All these data suggest that Sites IODP U1352, ODP 1119 and DSDP 594 were not fully covered by STW, but instead by an STW–SAW mixture during MIS 11c, MIS 7a–c and MIS 5e.

Similarly, the minimum proportion of *Nq. pachyderma* was also below 40% and *Gr. inflata* did not dominate over *Gg. bulloides* at IODP Site U1352 during MIS 7e (Fig. 5E, F), suggesting that the site might also have been covered by an STW–SAW mixture at that time. In contrast, at DSDP Site 594, the minimum proportion of *Nq. pachyderma* was above 40% during MIS 7e, implying that this site was covered by SAW. The above analysis allows us to infer that the southern edge of the SF was situated between IODP Site U1352 and DSDP Site 594 during MIS 7e.

In addition, the relative abundance of several more minor

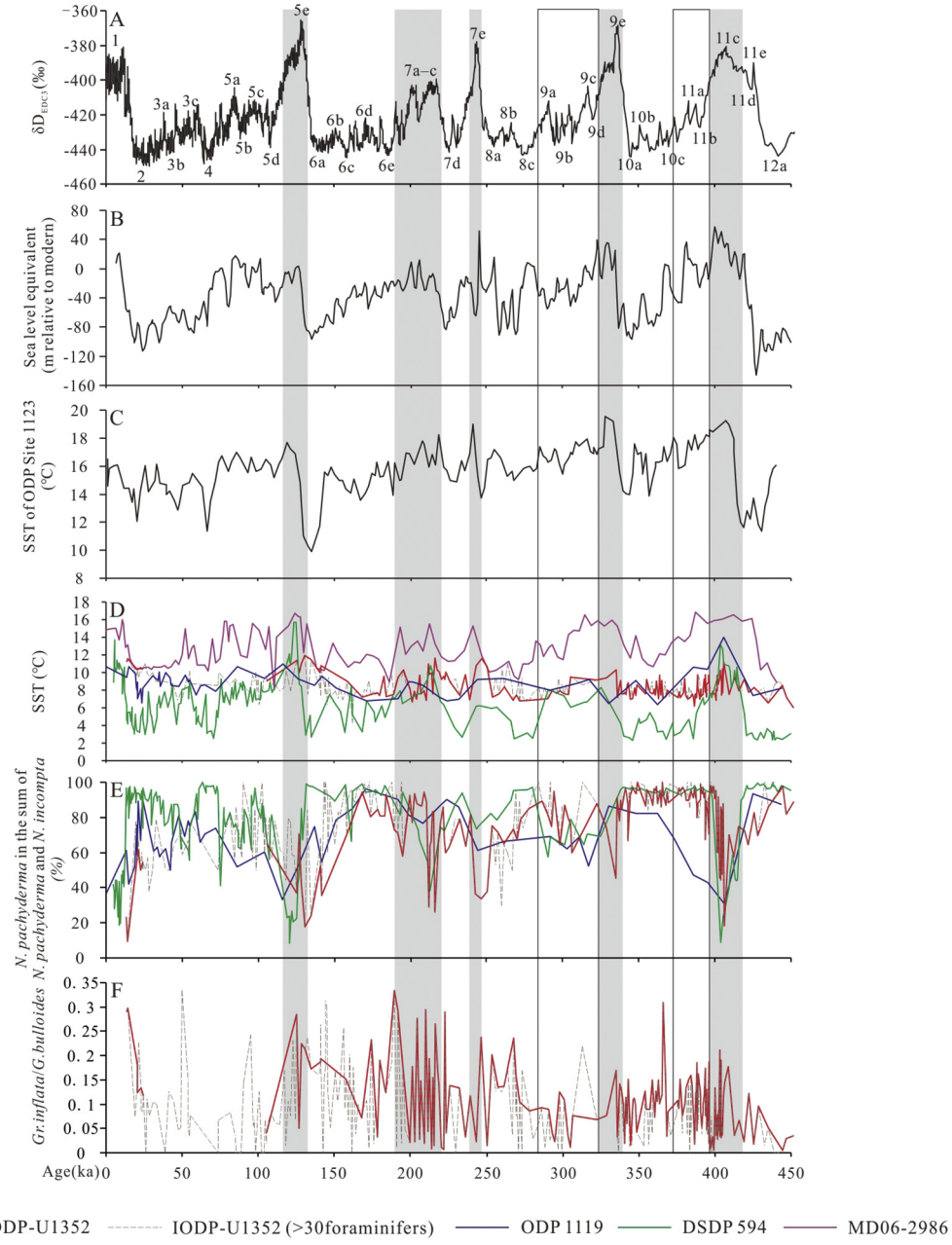

Fig. 5. (A) The EDC δD record on the AICC2012 time-scale (Bazin et al., 2013; Veres et al., 2013). (B) Sea level record of ODP Site 1123 (modified from Elderfield et al., 2012, positive numbers indicate sea level higher than today). (C) Sea surface temperature (SST) record of ODP Site 1123 (Crundwell et al., 2008). (D) Mean annual sea surface temperature estimates of Sites IODP U1352, ODP 1119, DSDP 594 and MD06-2986 for the last 450 kyr. (E) The percentage of *Nq. pachyderma* in the sum of *Nq. pachyderma* and *Nq. incompta* of Sites IODP-U1352, ODP 1119, and DSDP 594. (F) Ratio of *Gr. inflata* to *Gg. bulloides* curve of U1352B.

subtropical species such as *Gr. crassaformis* and *Gr. scitula* can be used to detect the influence of subtropical waters (King and Howard, 2001). The distinctively high abundances of *Gr. crassaformis* during MIS 11c, MIS 7e and MIS 7a–c (Fig. 3E), *Gr. scitula* and *Gr. crassula* during MIS 11c (Fig. 3H, I), and *Gr. truncatulinoides* during MIS 7e, MIS 7a–c and MIS 5e (Fig. 3G) point to the influence of STW at IODP Site U1352 during these interglacial periods. Note that, these species are all deep-dwelling species and thus we infer that the subtropical water body extended deeper during those periods than during MIS 11a–b and MIS 9a–d.

The location of IODP Site U1352 is currently covered by the SC and has a mean annual SST of 11 °C (Table 1). The reconstructed SSTs of U1352B during MIS 11c, MIS 7e, MIS 7a–c, and MIS 5e were relatively warm and in the range of present-day SST, with temperature maxima of 11.2, 11.6, 11.7, and 11.9 °C, respectively (Figs. 4 and 5). This suggests that the region was influenced by the same water mass during all those periods (Wilson et al., 2005). Furthermore, the SSTs of DSDP Site 594 during MIS 11c, MIS 7a–c, and MIS 5e were close to or slightly warmer than those of IODP Site U1352 (Figs. 4 and 5) while the SSTs of ODP Site 1119 during MIS 11c appeared similar to those of DSDP Site 594 (Wilson et al., 2005). Note that the low sampling resolution in ODP Site 1119 may have failed to capture the peaks in MIS 7e, MIS 7a–c, and MIS 5e. Thus, according to the results of the planktonic species, the SST records of U1352B, ODP 1119 and DSDP 594 support the notion that an STW–SAW mixture covered the three sites during MIS 11c, MIS 7a–c and MIS 5e, and in addition IODP Site U1352 during MIS 7e.

As the SF location is controlled by both the bathymetry and the climate, we compare the results of IODP Site U1352 with ODP Site 1123

(Crundwell et al., 2008) and the EDC δD record (on AICC2012 timescale; Jouzel et al., 2007; Bazin et al., 2013; Veres et al., 2013), to discuss the mechanism and the relationship between global climate change and SF migration. ODP Site 1123 is located on the Chatham Rise, east of New Zealand (Fig. 1, Table 1). With hydrographic effects considered minimal at this site (Past Interglacials Working Group of PAGES, 2016), ODP Site 1123 provides important insights into climate changes in the study region.

In the EDC δD record (Jouzel et al., 2007), MIS 11c, MIS 7e, and MIS 5e were the most prominent interglacial intervals, followed by MIS 7a–c (Fig. 5A). The SSTs of ODP Site 1123 (Crundwell et al., 2008) showed that MIS 11c and MIS 7e were obviously the most prominent interglacial periods in the study region, and were followed by MIS 7a–c and MIS 5e (Fig. 5C). Pelejero et al. (2006) inferred that the exceptional warming during MIS 11 might have characterised certain locations but was not global in nature. However, the SSTs estimated for MIS 11 to the southeast of Tasmania (FR1/94-GC3) are equal to those to the east of New Zealand (King and Howard, 2000), indicating that MIS 11 was comparable to today in the study region (Pelejero et al., 2006). In addition, Past Interglacials Working Group of PAGES (2016) concluded that MIS 11c and MIS 5e are consistently the strongest interglacial periods of the last 450 kyr. Therefore, it is possible that the warm climate during MIS 11c and MIS 5e made the STF move further southward than during MIS 11a–b and MIS 9a–d. This would result in an offshore movement of the SF.

The SSTs of IODP Site U1352 during MIS 7a–c were equal to MIS 11c and MIS 7e (Figs. 4 and 5). Although the EDC δD record (Jouzel et al., 2007; Bazin et al., 2013; Veres et al., 2013) indicated that MIS 7a–c were not as warm as MIS 11c and MIS 5e (Fig. 5A), both the SSTs of ODP Site 1123 (Crundwell et al., 2008) and core MD06-2986 (Hayward et al., 2012) showed that MIS 7a–c levels were similar to or slightly lower than MIS 11c and MIS 5e (Fig. 5C, D). Furthermore, the SSTs of DSDP Site 594 (Wilson et al., 2005) during MIS 7a–c were not as high as during MIS 11c and MIS 5e but higher than during MIS 7e and MIS 9e. Thus, the distinct warm climate in the study region during MIS 7a–c would be responsible for the offshore migration of the SF and resulted in an STW–SAW mixture affecting the three sites of IODP U1352, ODP 1119 and DSDP 594.

In the EDC δD record (Jouzel et al., 2007), MIS 7e was as warm as MIS 11c and MIS 5e (Fig. 5A). However, the SSTs of IODP Site U1123 during MIS 7e varied and were lower during the early stage when the sea level (Elderfield et al., 2012) was relatively high (Fig. 5C, B). The higher sea level might be responsible for the limited offshore migration of the SF during this period, hence the SF was situated between IODP Site U1352 and DSDP Site 594.

The planktonic foraminiferal assemblage and SST records of Sites IODP U1352, ODP 1119 and DSDP 594 during MIS 9e showed no evidence of any STW–SAW mixture influencing this region. If these data did not miss the signal of any STW–SAW mixture due to the temporal resolution, Sites IODP U1352, ODP 1119 and DSDP 594 should be covered by SAW then. Sea-level in the study region during MIS 9e was ~30 m higher than during MIS 7a–c, and MIS 5e, but was lower than during MIS 11c (Fig. 5B). As the climate during MIS 9e is unlikely to equal the most prominent MIS 11c, we infer that the coastward migration of the SF during this period was mainly caused by the higher sea-level.

5.1.2. MIS 11a–b and MIS 9a–d

The mean annual SSTs of Sites IODP U1352, ODP 1119 and DSDP 594 during MIS 11a–b and MIS 9a–d were similar and ~2 °C lower than those during MIS 11c, MIS 7a–c, and MIS 5e (Figs. 4 and 5). Moreover, the location of core MD06–2986 was always covered by STW during MIS 11, MIS 9, MIS 7 and MIS 5e (Hayward et al., 2012). The temperature differences between the three sites and core MD06-2986 during MIS 11a–b and MIS 9a–d (about 6 °C) were larger than during MIS 11c, MIS 7a–c, and MIS 5e (about 4 °C) (Figs. 4 and 5). Thus, Sites IODP U1352, ODP 1119 and DSDP 594 should be influenced by SAW during MIS 11a–b and MIS 9a–d. According to the analysis by Past Interglacials Working Group of PAGES (2016), MIS 11a–b and MIS 9a–d are not interglacial periods. The SSTs of ODP Site 1123 (Crundwell et al., 2008), and the EDC δD record (Jouzel et al., 2007; Bazin et al., 2013; Veres et al., 2013) (Fig. 5C, A) also showed that MIS 11a–b and MIS 9a–d were not as warm as MIS 11c, MIS 7e, MIS 7a–c, and MIS 5e. Thus, the southward migration of the STF caused by the warm climate during MIS 11a–b and MIS 9a–d was smaller than during MIS 11c, MIS 7e, MIS 7a–c, and MIS 5e. It failed to offset the sea-level steering that may have caused the SF to move coastward, and SAW influenced Sites IODP U1352, ODP 1119 and DSDP 594 during MIS 11a–b and MIS 9a–d.

5.2. Position of the Southland front and migration in glacial periods

The SSTs of IODP Site U1352 were very close to those of ODP Site 1119, and ~3–4 °C higher than those of DSDP Site 594 during MIS 7d and the glacial periods of MIS 10, MIS 8, and MIS 6 (Figs. 4 and 5). IODP Site U1352 is located 0.59° further north of DSDP Site 594, and ODP Site 1123 0.75° north of ODP Site 1125 (Fig. 1). The SST of ODP Site 1123 was only ~1–3 °C higher than at ODP Site 1125 during the glacial period when they were influenced by the same water mass (Hayward et al., 2008). Thus, the ~3–4 °C warmer SSTs at Sites IODP U1352 and ODP 1119 than at DSDP Site 594 were not caused only by the difference in latitude but also by the different prevailing surface-water masses, suggesting that the SF was situated between DSDP Site 594 and Sites IODP U1352, ODP 1119 during MIS 7d, MIS 10, MIS 8, and MIS 6. Site MD06-2986 was always covered by STW (Hayward et al., 2012) and IODP Site U1352 was influenced by the STW–SAW mixture during MIS 7d, MIS 10, MIS 8, and MIS 6, and interglacial periods of MIS 11c, MIS 7e, MIS 7a–c, and MIS 5e. Thus, the temperature differences (~4 °C) between IODP Site U1352 and core MD06-2986 during MIS 7d, MIS 10, MIS 8, and MIS 6 were like the differences (~4–5 °C) during MIS 11c, MIS 7e, MIS 7a–c, and MIS 5e (Figs. 4 and 5). We therefore conclude that during MIS 7d and the glacial periods of MIS 10, MIS 8, and MIS 6, the lowered sea-level caused the SF to migrate offshore. Sites IODP U1352 and ODP 1119 were covered by the STW–SAW mixture and DSDP Site 594 by the SAW. Hence, unlike the previous studies, our results identify MIS 7d as a glacial period in the study region. This agrees with the conclusion of Past Interglacials Working Group of PAGES (2016).

6. Conclusions

Comparisons of the SST records of IODP Site U1352 with those of ODP Site 1119, DSDP Site 594 and core MD06-2986 reveal the movement of the surface water masses off the east coast of the South Island over the last 450 kyr.

The seaward migration of the Southland Front, a dynamic and sensitive section of the Subtropical Front in the south-west Pacific, during MIS 11c, MIS 7a–c, and MIS 5e caused an STW–SAW mixture to influence Sites IODP U1352, ODP 1119 and DSDP 594. The Southland Front also migrated seaward during MIS 7e with its southern edge located between IODP Site U1352 and DSDP Site 594.

Sites IODP U1352, ODP 1119 and DSDP 594 recorded a coastward migration of the Southland Front during MIS 11a–b and MIS 9a–d, and the three sites were covered by SAW during these periods.

The Southland Front migrated offshore during MIS 7d and glacial periods of MIS 10, MIS 8, and MIS 6, its southern edge was located between DSDP Site 594 and Sites IODP U1352, ODP 1119. MIS 7d is identified as a glacial period in the study region.

Acknowledgements

Samples were taken by Integrated Ocean Drilling Program

Expedition 317. We are grateful to the shipboard participants in IODP Expedition 317 for their hard work. We thank Allan Chivas of University of Wollongong and Liping Zhou of Peking University for suggestions. We also thank Prof. Richard Jordan and two anonymous reviewers for their critical remarks and constructive suggestions. This work was supported by the National Natural Science Foundation of China (41176055).

References

Barrows, T.T., Juggins, S., De Deckker, P., Theide, J., Martinez, J.I., 2000. Sea-surface temperatures of the Southwest Pacific Ocean during the last glacial maximum. Paleoceanography 15 (1), 95–109.

Bazin, L., Landais, A., Lemieux-Dudon, B., Toye Mahamadou Kelé, H., Veres, D., Parrenin, F., Martinerie, P., Ritz, C., Capron, E., Lipenkov, V., Loutre, M.F., Raynaud, D., Vinther, B., Svensson, A., Rasmussen, S.O., Severi, M., Blunier, T., Leuenberger, M., Fischer, H., Masson-Delmotte, V., Chappellaz, J., Wolff, E., 2013. An optimized multi-proxy, multi-site Antarctic ice and gas orbital chronology (AICC2012): 120–800 ka. Clim. Past 9, 1715–1731.

Bé, A.W.H., 1977. An ecological, zoogeographic and taxonomic review of recent planktonic foraminifera. In: Ramsay, A.T.S. (Ed.), Oceanic Micropaleontology. vol. 1. Academic Press, London, pp. 1–100.

Bé, A.W.H., Tolderlund, D.S., 1971. Distribution and ecology of living planktonic foraminifera in surface waters of the Atlantic and Indian Oceans. In: Funnell, B.M., Riedel, W.R. (Eds.), The Micropaleontology of Oceans. Cambridge University Press, New York, pp. 105–149.

Brock, J.C., McClain, C.R., Anderson, D.M., Prell, W.L., Hay, W.W., 1992. Southwest monsoon circulation and environments of recent planktonic foraminifera in the northwestern Arabian Sea. Paleoceanography 7 (6), 799–813.

Capotondi, L., Girone, A., Lirer, F., 2016. Central Mediterranean mid-Pleistocene paleoclimatic variability and its association with global climate. Palaeogeogr. Palaeoclimatol. Palaeoecol. 442, 72–83.

Carter, R.M., 2005. A New Zealand climatic template back to c. 3.9 Ma: ODP site 1119, Canterbury bight, south-west Pacific Ocean, and its relationship to onland successions. J. R. Soc. N. Z. 35, 9–42.

Carter, R.M., Gammon, P.R., 2004. New Zealand maritime glaciation: millennial scale southern climate change since 3.9 Ma. Science 304, 1659–1662.

Carter, R.M., Gammon, P.R., Millwood, L., 2004. Glacial-interglacial (MIS 1–10) migrations of the subtropical front across ODP site 1119, Canterbury bight, Southwest Pacific Ocean. Mar. Geol. 205, 29–58.

Chiswell, S.M., Bostock, H.C., Sutton, P.J.H., Williams, M.J.M., 2015. Physical oceanography of the deep seas around New Zealand: a review. N. Z. J. Mar. Freshw. Res. 49 (2), 286–317.

Clare, G.R., Fitzharris, B.B., Chinn, T.J., Salinger, M.J., 2002. Interannual variation in end-of-summer snowlines of the southern alps of New Zealand, and relationships with southern hemisphere atmospheric circulation and sea surface temperature patterns. Int. J. Climatol. 22, 107–120.

Cléroux, C., deMenocal, P., Arbuszewski, J., Linsley, B., 2013. Reconstructing the upper water column thermal structure in the Atlantic Ocean. Paleoceanography 28, 503–516.

Crundwell, M., Scott, G., Naish, T., Carter, L., 2008. Glacial-Interglacial Ocean climate variability from planktonic foraminifera during the mid-Pleistocene transition in the temperate Southwest Pacific, ODP site 1123. Palaeogeogr. Palaeoclimatol. Palaeoecol. 260, 202–229.

Cullen, J.L., 1981. Microfossil evidence for changing salinity patterns in the bay of Bengal over the last 20 000 years. Palaeogeogr. Palaeoclimatol. Palaeoecol. 35, 315–356.

Dieckmann, G.S., Spindler, M., Lange, M.A., Ackley, S.F., Eicken, H., 1991. Antarctic Sea ice: a habitat for the foraminifer *Neogloboquadrina pachyderma*. J. Foraminifer. Res. 21 (2), 181–194.

Ding, X., Wu, Y.-Y., Li, W., 2017. A new 0.9 Ma oxygen isotope stratigraphy for a shallow-water sedimentary transect across three IODP 317 sites in the Canterbury bight of Southwest Pacific Ocean. Palaeogeogr. Palaeoclimatol. Palaeoecol. 465, 1–13.

Duplessy, J.C., Bé, A.W.H., Blanc, P.L., 1981. Oxygen and carbon isotopic composition and biogeographic distribution of planktonic foraminifer in the Indian Ocean. Palaeogeogr. Palaeoclimatol. Palaeoecol. 33, 9–46.

Elderfield, H., Ferretti, P., Greaves, M., Crowhurst, S., McCave, I.N., Hodell, D., Piotrowski, A.M., 2012. Evolution of ocean temperature and ice volume through the mid-Pleistocene climate transition. Science 337, 704–709.

Site U1352. In: Expedition 317 Scientists, Fulthorpe, C.S., Hoyanagi, K., Blum, P., the Expedition 317 Scientists (Eds.), Proceedings of the Integrated Ocean Drilling Program. Vol. 317. Integrated Ocean Drilling Program Management International Press, Tokyo, pp. 1–171.

Fenner, J., Carter, L., Stewart, R.B., 1992. Late quaternary paleoclimatic and paleogeographic change over the northern Chatham rise. Mar. Geol. 108, 383–404.

Hayward, B.W., Scott, G.H., Crundwell, M.P., Kennett, J.P., Cater, L., Neil, H.L., Sabaa, A.T., Wilson, K., Rodger, J.S., Schaefer, G., Grenfell, H.R., Li, Q.-Y., 2008. The effect of submerged Plateaux on Pleistocene gyral circulation and sea-surface temperatures in the Southwest Pacific. Glob. Planet. Chang. 63, 309–316.

Hayward, B.W., Sabaa, A.T., Kolodziej, A., Crundwell, M.P., Steph, S., Scott, G.H., Neil, H.L., Bostock, H.C., Carter, L., Grenfell, H.R., 2012. Planktic foraminifera-based sea-surface temperature record in the Tasman Sea and history of the subtropical front around New Zealand, over the last one million years. Mar. Micropaleontol. 82–83, 13–27.

Heath, R.A., 1972. The Southland current. N. Z. J. Mar. Freshw. Res. 6, 497–533.

Heath, R.A., 1985. A review of the physical oceanography of the seas around New Zealand — 1982. N. Z. J. Mar. Freshw. Res. 19, 79–124.

Hemleben, C., Spindler, M., Anderson, O.R., 1989. Modern Planktonic Foraminifera. Springer-Verlag, New York.

Hoyanagi, K., Kawagata, S., Koto, S., Kamihashi, T., Ikehara, M., 2014. Data report: Pleistocene benthic foraminiferal oxygen and stable carbon isotopes and their application for age models, Hole U1352, offshore New Zealand. In: Fulthorpe, C.S., Hoyanagi, K., Blum, P., the Expedition 317 Scientists (Eds.), Proceedings of the Integrated Ocean Drilling Program. Integrated Ocean Drilling Program Management International, Inc, Tokyo, pp. 317.

Imbrie, J., Kipp, N.G., 1971. A new micropaleontological method for paleoclimatology: application to a Late Pleistocene Caribbean core. In: Turekian, K.K. (Ed.), The Late Cenozoic Glacial Ages. Yale University Press, New Haven, pp. 71–131.

Johannessen, T., Jansen, E., Flatøy, A., Ravelo, A.C., 1994. The relationship between surface watermasses, oceanographic fronts and paleoclimatic proxies in surface sediments of the Greenland, Iceland, Norwegian seas. In: Zahn, R., Pedersen, T.F., Kaminski, M.A., Labeyrie, L. (Eds.), Carbon Cycling in the Glacial Ocean: Constraints on the Ocean's Role in Global Change. vol. 17 of the series NATO ASI Series. Springer-Verlag Press, Berlin, pp. 61–85.

Jouzel, J., Masson-Delmotte, V., Cattani, O., Dreyfus, G., Falourd, S., Hoffmann, G., Minster, B., Nouet, J., Barnola, J.M., Chappellaz, J., Fischer, H., Gallet, J.C., Johnsen, S., Leuenberger, M., Loulergue, L., Luethi, D., Oerter, H., Parrenin, F., Raisbeck, G., Raynaud, D., Schilt, A., Schwander, J., Selmo, E., Souchez, R., Spahni, R., Stauffer, B., Steffensen, J.P., Stenni, B., Stocker, T.F., Tison, J.L., Werner, M., Wolff, E.W., 2007. Orbital and millennial Antarctic climate variability over the past 800,000 years. Science 317, 793–796.

King, A.L., Howard, W.R., 2000. Middle Pleistocene Sea-surface temperature change in the Southwest Pacific Ocean on orbital and suborbital time scales. Geology 28, 659–662.

King, A.L., Howard, W.R., 2001. Seasonality of foraminiferal flux in sediment traps at Chatham rise, SW Pacific: implications for paleotemperature estimates. Deep Sea Res. Part I 48 (7), 1687–1708.

King, A.L., Howard, W.R., 2003. Planktonic foraminiferal flux seasonality in Subantarctic sediment traps: a test for palaeoclimate reconstructions. Paleoceanography 18 (1), 1019.

Kipp, N.G., 1976. New transfer function for estimating past sea-surface conditions from seabed distribution of planktonic foraminiferal assemblages in the North Atlantic. In: Cline, R.M., Hays, J.D. (Eds.), Investigation of Late Quaternary Paleoceanography and Paleoclimatology. Vol. 145. Geological Society of America Memoir, pp. 3–42.

Kucera, M., 2007. Planktonic Foraminifera as Tracers of Past Oceanic Environments. Developments in Marine Geology. Vol. 1. pp. 213–262.

Kucera, M., Weinelt, M., Kiefer, T., Pflaumann, U., Hayes, A., Weinelt, M., Chen, M.-T., Mix, A.C., Barrows, T.T., Cortijo, E., Duprat, J., Juggins, S., Waelbroeck, C., 2005. Reconstruction of sea-surface temperatures from assemblages of planktonic foraminifera: multi-technique approach based on geographically constrained calibration data sets and its application to glacial Atlantic and Pacific Ocean. Quat. Sci. Rev. 24, 951–998.

Le, J., Shackleton, N.J., 1992. Carbonate dissolution fluctuations in the western equatorial Pacific during the late quaternary. Paleoceanography 7, 21–42.

Li, W.-B., Wang, R.-J., Xiang, F., Ding, X.-H., Zhao, M.-X., 2010. Sea surface temperature and subtropical front movement in the South Tasman Sea during the last 800 ka. Chin. Sci. Bull. 55 (29), 3338–3344.

Lisiecki, L.E., Raymo, M.E., 2005. A Pliocene-Pleistocene stack of 57 globally distributed benthic $\delta^{18}O$-records. Paleoceanography 20, PA1003.

Marret, F., De Vernal, A., Benderra, F., Harland, R., 2001. Late quaternary sea-surface conditions at DSDP hole 594 in the Southwest Pacific Ocean based on dinoflagellate cyst assemblages. J. Quat. Sci. 16 (7), 739–751.

Martinez, J.I., Taylor, L., De Deckker, P., Barrows, T., 1998. Planktonic foraminifera from the eastern Indian Ocean: distribution and ecology in relation to the western Pacific warm pool (WPWP). Mar. Micropaleontol. 34, 121–151.

Nelson, C.S., Cooke, P.J., Hendy, C.H., Cuthbertson, A.M., 1993. Oceanographic and climatic changes over the past 160,000 years at the Deep Sea drilling project site 594 off southeastern New Zealand, Southwest Pacific Ocean. Paleoceanography 8 (4), 435–458.

Nelson, C.S., Hendy, I.L., Neil, H.L., Hendy, C.H., Weaver, P.P.E., 2000. Last glacial jetting of cold waters through the subtropical convergence zone in the Southwest Pacific off eastern New Zealand, and some geological implications. Palaeogeogr. Palaeoclimatol. Palaeoecol. 156, 103–121.

Niebler, H.S., Gersonde, R., 1998. A planktic foraminiferal transfer function for the southern South Atlantic Ocean. Mar. Micropaleontol. 34, 213–234.

Niebler, H.S., Arz, H.W., Donner, B., Mulitza, S., Pätzold, J., Wefer, G., 2003. Sea surface temperatures in the equatorial and South Atlantic Ocean during the last glacial maximum (23–19 ka). Paleoceanography 18 (3), 1069.

Oerlemans, J., Fortuin, J.P.F., 1992. Sensitivity of glaciers and small ice caps to greenhouse warming. Science 258, 115–117.

Pahnke, K., Zahn, R., Elderfield, H., Schulz, M., 2003. 340,000-year centennial scale marine record of southern hemisphere climatic oscillation. Science 301, 948–952.

Parker, F.L., 1962. Planktonic foraminifera species in Pacific sediments. Micropaleontology 8, 219–254.

Parker, F.L., Berger, W.H., 1971. Faunal and solution patterns of planktonic foraminifera in surface sediments of the South Pacific. Deep-Sea Res. 18, 73–107.

Past Interglacials Working Group of PAGES, 2016. Interglacials of the last 800,000 years. Rev. Geophys. 54, 162–219. http://dx.doi.org/10.1002/2015RG000482.

Pelejero, C., Calvo, E., Barrows, T.T., Logan, G.A., De Deckker, P., 2006. South Tasman Sea alkenone palaeothermometry over the last four glacial/interglacial cycles. Mar.

Geol. 230, 73–86.
Pflaumann, U., Jian, Z., 1999. Modern distribution patterns of planktonic foraminifera in the South China Sea and western Pacific: a new transfer technique to estimate regional sea-surface temperatures. Mar. Geol. 156, 41–83.
Pflaumann, U., Duprat, J., Pujol, C., Labeyrie, L.D., 1996. SIMMAX: a modern analog technique to deduce Atlantic Sea surface temperatures from planktonic foraminifera in deep-sea sediments. Paleoceanography 11 (1), 15–35.
Prell, W.L., Curry, W.B., 1981. Faunal and isotope indices of monsoonal upwelling: western Arabian Sea. Oceanol. Acta 4, 91–98.
Prell, W., Martin, A., Cullen, J., Trend, M., 1999. The Brown University Foraminiferal Data Base, IGBP PAGES/World Data Center-A for Paleoclimatology Data Contribution Series # 1999-02. NOAA/NGDC Paleoclimatology Program, Boulder, CO, U. SA. www1.ncdc.noaa.gov/pub/data/paleo/paleocean/brown_foram/ (3/11/2017).
Railsback, L.B., Gibbard, P.L., Head, M.J., Voarintsoa, N.R.G., Toucanne, S., 2015. An optimized scheme of lettered marine isotope substages for the last 1.0 million years, and the climatostratigraphic nature of isotope stages and substages. Quat. Sci. Rev. 111, 94–106.
Reynolds, L.A., Thunell, R.C., 1986. Seasonal production and morphologic variation of *Neogloboquadrina pachyderma* (Ehrenberg) in the Northeast Pacific. Micropaleontology 32 (1), 1–18.
Sabaa, A.T., Sikes, E.L., Hayward, B.W., Howard, W.R., 2004. Pliocene Sea surface temperature changes in ODP site 1125, Chatham rise, east of New Zealand. Mar. Geol. 205, 113–125.
Schaefer, G., Rodger, J.S., Hayward, B.W., Kennett, J.P., Sabaa, A.T., Scott, G.H., 2005. Planktic foraminiferal and sea surface temperature record during the last 1 Myr across the subtropical front Southwest Pacific. Mar. Micropaleontol. 54, 191–212.
Scott, G.H., Hall, I.R., 2004. Planktonic foraminiferal evidence on late Pliocene-quaternary near surface water masses at ODP site 1123B, northern Chatham rise, east of New Zealand. Mar. Geol. 205, 127–145.
Shaw, A.G.P., Vennell, R., 2000. Variability of water masses through the Mernoo saddle, South Island, New Zealand. N. Z. J. Mar. Freshw. Res. 34, 103–116.
Sikes, E.L., Howard, W.R., Neil, H.L., Volkman, J.K., 2002. Glacial-interglacial sea surface temperature changes across the subtropical front east of New Zealand based on alkenone unsaturation ratios and foraminiferal assemblages. Paleoceanography 17 (2), 2-1–2-13.
Sutton, P.J.H., 2003. The Southland current: a subantarctic current. N. Z. J. Mar. Freshw. Res. 37, 645–652.
Thiede, J., Nees, S., Schulz, H., DeDeckker, P., 1997. Oceanic surface conditions recorded on the sea floor of the Southwest Pacific Ocean through the distribution of foraminifers and biogenic silica. Palaeogeogr. Palaeoclimatol. Palaeoecol. 131, 207–239.
Thunell, R.C., Reynolds, L.A., 1984. Sedimentation of planktonic foraminifera: seasonal changes in species flux in the Panama Basin. Micropaleontology 30 (3), 243–262.
Tolderlund, D.S., Bé, A.W.H., 1971. Seasonal distribution of planktonic foraminifera in the western North Atlantic. Micropaleontology 17 (3), 297–329.
Veres, D., Bazin, L., Landais, A., Toyé Mahamadou Kele, H., Lemieux-Dudon, B., Parrenin, F., Martinerie, P., Blayo, E., Blunier, T., Capron, E., Chappellaz, J., Rasmussen, S.O., Severi, M., Svensson, A., Vinther, B., Wolff, E.W., 2013. The Antarctic ice core chronology (AICC2012): an optimized multi-parameter and multi-site dating approach for the last 120 thousand years. Clim. Past 9, 1733–1748.
Weaver, P.P.E., Neil, H., Carter, L., 1997. Sea surface temperature estimates from the Southwest Pacific based on planktonic foraminifera and oxygen isotopes. Palaeogeogr. Palaeoclimatol. Palaeoecol. 131, 241–256.
Weaver, P.P.E., Carter, L., Neil, H.L., 1998. Response of surface water masses and circulation to late quaternary climate change east of New Zealand. Paleoceanography 13 (1), 70–83.
Wells, P., Okada, H., 1997. Response of nannoplankton to major changes in sea-surface temperature and movements of hydrological fronts over site DSDP site 594 (South Chatham rise, southeastern New Zealand), during the last 130 kyr. Mar. Micropaleontol. 32, 341–363.
Wilson, K., Hayward, B.W., Sabaa, A.T., Scott, G.H., Kennett, J.P., 2005. A one-million-year history of a north-south segment of the subtropical front, east of New Zealand. Paleoceanography 20, PA2004. https://www.nodc.noaa.gov/cgi-bin/OC5/woa13/woa13.pl (web archive link, 11 March 2017) 3/11/2017. http://paleosofttools.usal.es.